

学位論文

Molecular Tips for Chemically Selective STM

分子探針による化学選択性 STM

平成 16 年 1 月博士（理学）申請

東京大学大学院理学系研究科

化学専攻

西野 智昭

Acknowledgement

I would like to be most grateful to Prof. Dr. Yoshio Umezawa for the opportunity to work on this exciting project together with his invaluable discussion, useful suggestions, and profound support.

I wish to be thankful to Dr. Takashi Ito for his invaluable discussion and profitable advice.

I would like to appreciate Prof. Dr. Masaru Tsukada, Dr. Katsunori Tagami (Department of Physics, Faculty of Science, The University of Tokyo), and Dr. Nobuyuki Isshiki (Materials Development Research Laboratories, Kao Corporation) for their illuminating discussion on imaging mechanism of STM using molecular tips.

Further thanks go to: Dr. Hiroshi Aoki for his daily suggestive discussion and advice that contains scientific issues and daily matters. Mr. Takahito Ohshiro for his incessant discussion and advice. All other students of Prof. Umezawa's laboratory for their kind assistance.

Abstract

Scanning tunneling microscopy (STM) has been a powerful tool in surface science. STM, however, often lacks chemical selectivity. In this laboratory, it has been demonstrated that the use of molecular tips allows STM to attain the chemical selectivity. The chemical selectivity arises from the facilitation of electron tunneling by chemical interactions between tip molecules and particular chemical species of sample molecules. The available interactions reported so far include hydrogen bond and metal-coordination interactions.

In the present study, I showed facilitation of electron tunneling through charge-transfer interaction, which allows us to locate electroactive moieties and to construct a novel intermolecular junction for testing molecular-scale electronic devices. In addition, it was demonstrated that carboxy-terminated single-walled carbon nanotube (SWNT) tips enable high resolution and chemically selective observation. Finally, it was shown that the selective observation of oxygen-containing functional groups can be tailored by controlling the extent of the hydrogen bond acidity or basicity of tip molecules.

Table of Contents

1.	General Introduction	8
2.	STM and Use of Molecular Tips	12
2.1.	Fundamentals	12
2.1.1.	Operating principle	12
2.1.2.	Theories of STM	13
2.1.3.	Thin organic layers	19
2.2.	Molecular Tips	20
2.2.1.	Analogy between electrochemistry and STM	20
2.2.2.	Chemical modification of STM tips	22
2.2.3.	Discrimination of functional groups based on hydrogen bond interactions	24
2.2.4.	Orientation-sensitive observation of ether oxygens	30
2.2.5.	Polypyrrole tips	34
2.2.6.	Discrimination of metal ions of porphyrins based on metal-coordination and hydrogen bond interactions	36
3.	A Fullerene Molecular Tip: Locating Electroactive Moieties	

and a Novel Intermolecular Junction for Molecular Electronics

3.1.	Introduction	40
3.2.	Experimental Section	43
3.2.1.	General	43
3.2.2.	Synthesis of <i>N</i> -methyl 2-(2-propyldithiophenyl)fulleropyrro- lidine (MPF)	44
3.2.3.	STM tip preparation	44
3.2.4.	STM observation of MPF SAMs	45
3.2.5.	STM observation of physisorbed monolayers of the porphyrins	45
3.3.	Results	46
3.3.1.	Tip modification	46
3.3.2.	CoPor monolayer	48
3.3.3.	Mixed monolayer of FBPor and ZnPor	52
3.4.	Discussion	54
3.4.1.	Imaging mechanism	54
3.4.2.	Polarity dependence	57
3.5.	Conclusions	58

4.	Carboxy-Terminated Carbon Nanotube Tips	60
4.1.	Introduction	60
4.2.	Experimental Section	62
4.2.1.	Reagents	63
4.2.2.	Tip modification	63
4.2.3.	STM observation	64
4.2.4.	Transmission electron microscopy (TEM) observation	65
4.3.	Results and Discussion	65
4.4.	Conclusions	71
5.	Control of the Chemical Selectivity	72
5.1.	Introduction	72
5.2.	Experimental	74
5.2.1.	Reagents	75
5.2.2.	Tip preparation	76
5.2.3.	STM observations	76
5.3.	Results	78
5.3.1.	Unmodified tips	78
5.3.2.	4MP tips	79
5.3.3.	4MBSA tips	81

5.3.4.	4MBA tips	82
5.3.5.	TP tips	82
5.4.	Discussion	83
5.5.	Conclusions	85
6.	General Conclusions	87
7.	References	90

1. General Introduction

Soon after its invention, scanning tunneling microscopy (STM) successfully revealed the atomic arrangement on the reconstructed surface of silicon crystals, which could not be strictly defined for a couple of decades. Since this, STM has been accepted as an attractive tool for surface science because of extremely high spatial resolution, ability for the observation at real space, and wide applicability under a variety of environments. On the other hand, one of the drawbacks of the STM is its lack of chemical selectivity.

In this laboratory, it has been demonstrated that the use of molecular tips allows STM to attain the chemical selectivity. The molecular tips were prepared by chemical modification of conventional metal tips, typically by self-assembled monolayers (SAMs) of aromatic thiols on gold tips. The outermost single molecular adsorbates probe the tunneling current flowing from or to a sample surface. The tunneling current significantly increases when chemical interaction is formed between tip and sample because electron tunneling is facilitated by electronic coupling brought by the interaction. A

certain moiety of a sample molecule that interacts with a tip molecule is, as a result, selectively observed as a bright spots in the STM image. The available chemical interactions reported so far include hydrogen bond and metal-coordination bond interactions.

In Chapter 2, fundamentals of STM are briefly described. In addition to this, the studies on molecular tips reported so far from this laboratory were summarized.

Because the overlap of electronic wave functions is important for the facilitation of intermolecular electron tunneling between tip and sample, the previous studies suggest that the electron tunneling should be facilitated also through the remaining electronic interaction, namely, a charge-transfer interaction in addition to the hydrogen bond and metal-coordination interactions. Electron donors and acceptors, which form charge-transfer interaction with each other, constitute major components for molecular electronic devices, such as molecular wires, diodes, or switches. Both the spatial arrangement of the electroactive species and their electronic configuration

within the local environment are key factors to realize the device functions in a desired manner.

In Chapter 3, it was demonstrate that molecular tips allow us to pinpoint electron-donaing or -accepting moieties in single molecules based on facilitated electron tunneling through charge-transfer interaction. In addition, we observed asymmetric electron transport between donor and acceptor, indicating the possibility for the molecular tip to address the electronic properties of donor–acceptor assemblies.

In Chapter 4, the use of carboxy-terminated carbon nanotube (CNT) tips is presented. CNTs can be regarded as hollow cylinders with diameters of a few nanometers. In spite of their tiny dimensions, they are mechanically robust and buckle reversibly. In addition, the high electron conductivity of the CNTs is one of the characteristics that makes CNT an attractive material for use as the STM tips. It is demonstrated for the first time that the STM tips of single-walled carbon nanotubes (SWNTs), smaller CNTs than multi-walled carbon nanotubes and thus expected to allow higher resolution, can be prepared by a simple wet chemistry using a reported immobilization procedure of SWNTs onto a flat

solid surface. With these SWNT tips, it is demonstrated that the ether oxygens of sample can be selectively and highly reproducibly recognized at high resolution by facilitation of electron tunneling through hydrogen bond interaction between the ether oxygens and carboxyl groups at the apex of SWNTs.

Chapter 5 describes the control of the chemical selectivity attained with molecular tips upon differing extent of the chemical interaction between a tip and sample molecules. Molecular tips of 4-mercaptopyridine, 4-mercaptobenzenesulfonic acid, and 4-mercaptobenzoic acid were used for the STM observation of $\text{CH}_3(\text{CH}_2)_{20}\text{COO}(\text{CH}_2)_{16}\text{OH}$. The effect of the hydrogen bond acidity or basicity of the tip molecules on the chemical selectivity is discussed.

2. STM and Use of Molecular Tips

2.1. Fundamentals

2.1.1. Operating principle

When two metal surfaces face very closely to each other with bias voltage applied, electron flows between them. STM relies on this phenomenon, which is called electron tunneling, as an operating principle. In STM observation, one of these two surfaces is that of atomically sharp metal tip, and the other is sample surface. The tip is in close proximity of the order of 1 nm or less to the sample surfaces, and a certain voltage of the order of 1–2 V is applied in between. This results in the tunneling current flow of the order of 1–2 nA between them. Although the detailed expression of the tunneling current is presented in the next section, the current, I , might be roughly approximated by¹

$$I \approx \exp\left(-\frac{2z}{\lambda}\right)$$

where $\lambda = \frac{\hbar}{\sqrt{2m\phi}}$; and symbols are: \hbar Plank's constant; m the electron rest mass; ϕ the work function of the sample. The tunneling current thus depends on the distance z between the two surfaces. The exponential dependence of

the current on the distance between tip and sample surface provides the high resolution achieved by STM. The tip scans over the sample surface keeping either the distance (constant height mode) or the tunneling current (constant current mode) between the tip and sample to be constant. The modulation of the tunneling current and the distance between the tip and the surface is mapped at the constant height and current mode, respectively. Both of the two modulations reflect the topography of the sample surface as indicated by the equation above.

2.1.2. Theories of STM²

Soon after the invention, many studies have been performed with STM. And surprisingly clear atomic images of metal and semiconductor surfaces are reported as well as those of adsorbed atoms and molecules. On the other hand, the interpretation of STM images is not always trivial. In order to understand and to quantitatively analyze the observed images, it is essential to theoretically explain the mechanism of STM.

Early theoretical description of the tunneling current was initiated by Tersoff and Hamann (TH) based on perturbation theory.^{3,4} Because the distance

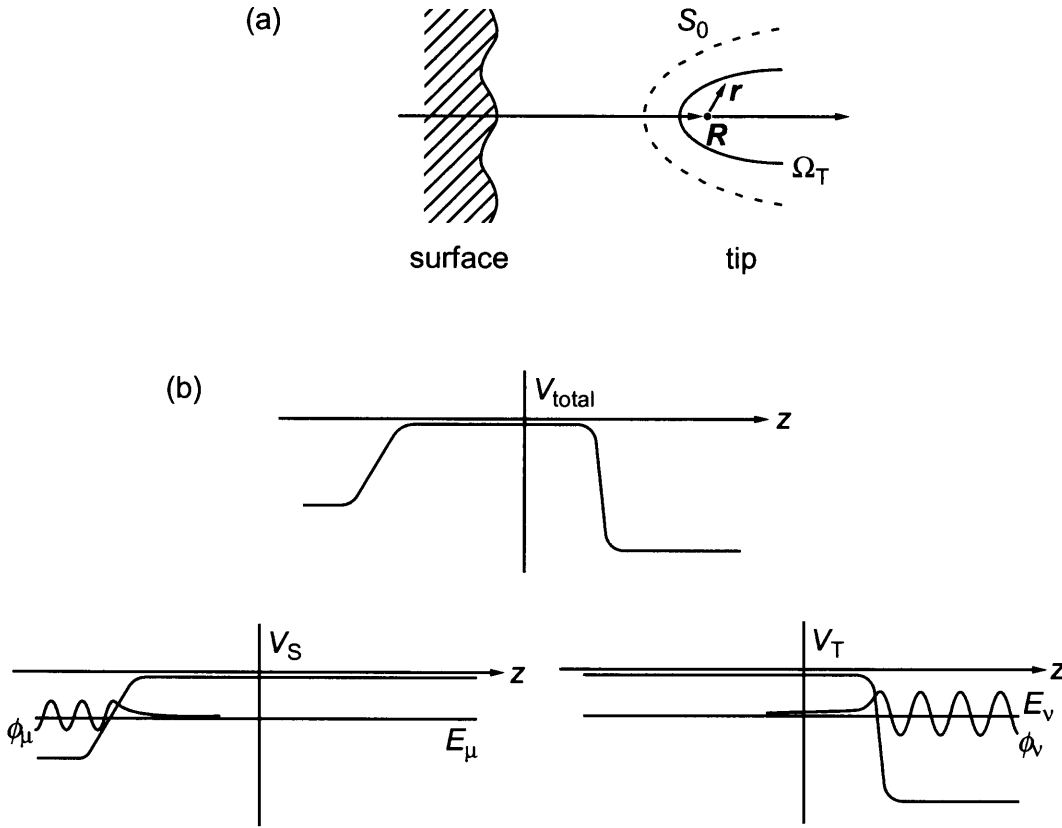


Fig. 2.1. (a) Geometry and (b) potential of the surface-tip system. (a) r is internal coordinate in the tip region Ω_T with reference to a certain fixed point R . (b) V_S and V_T are the potential of the surface and tip, respectively. ϕ_μ (ϕ_ν) and E_μ (E_ν) are the wave function and the corresponding eigen energy, respectively, of the surface (tip).

between the tip and surface is not very close (approximately several angstroms)

and the bias voltage is weak in STM observation, the tunnel Hamiltonian

method is valid for the description of the tunneling process. According to this

approach, Bardeen's equation for the tunneling current I is expressed as⁵

$$I = \frac{2\pi e}{\hbar} \sum_{\mu, \nu} [f(E_\mu) - f(E_\nu + eV)] |M_{\mu\nu}|^2 \delta(E_\mu - E_\nu), \quad (1)$$

where the tunneling matrix element is given by

$$M_{\mu\nu} = \frac{\hbar^2}{2m} \int_{S_0} dS (\phi_\mu^* \nabla \phi_\nu - \phi_\nu \nabla \phi_\mu^*). \quad (2)$$

In the above equations, ϕ_μ , E_μ (ϕ_ν , E_ν) are the eigen function and its corresponding eigen energy of the surface (tip) system, respectively. $f(E)$ is the Fermi distribution function and V is the bias voltage between tip and sample. In eq. (2), the integral is over any surface lying entirely within the gap region as shown in Fig. 2.1, and the quantity in parentheses is simply the current operator. Tersoff and Hamann used spherical-tip approximation to include only the s-type tip wave functions in evaluating the matrix element. With this assumption, they have deduced the expression of the tunnel current for the weak bias case,

$$I \propto V \rho(\mathbf{R}, E_F), \quad (3)$$

where $\rho(\mathbf{R}, E_F)$ is the local density of states (LDOS) of the surface at the center position \mathbf{R} of the spherical tip and at the Fermi level E_F . On the basis of this equation, the tunnel current is proportional to the LDOS and, importantly, can be related to a property of the surface in the absence of the tip.

Although the virtues of relation (1) have been more or less implicitly supposed for the analysis of most of the experimental data, the validity of the TH relation (3) is quite dependent on the electronic states of the tip because of

the crude approximation of the spherical-tip they used. If we extended the relation (3) for finite bias voltage, the following relation would be expected

$$\frac{dI}{dV} \propto \rho(\mathbf{R}, E_F - eV). \quad (4)$$

The derivative can be measured by scanning tunneling spectroscopy (STS), and eq. (4) has been more or less implicitly assumed in interpretation of STS data. However, negative differential resistance (NDR) behavior of STS is often observed in very small localized regions on sample surfaces.^{6,7} For the NDR, the electronic states of the tip is crucial, and the eq. (4) is not valid anymore to explain the NDR effect. It is thus needed to carefully model the microscopic nature of the tip. In the direction of TH approach, the generalized relation has been reported where p and d states as tip orbitals are used to calculate the corresponding tunnel matrix elements.⁸

Tsukada et al. have extended the perturbation approach to a realistic atomic model of the tip to derive more rigorous and general expression which replace the intuitive relation of the TH equation (3).² At first, the Bardeen's equation of the tunneling current (eq. (1)) is rewritten as

$$I = \frac{2\pi e}{\hbar} \int dE [f(E) - f(E + eV)] A(\mathbf{R}, E, E + eV), \quad (5)$$

where

$$A(\mathbf{R}, E, E') = \int_{\Omega_T} d\mathbf{r} \int_{\Omega_T} d\mathbf{r}' V_T(\mathbf{r}) V_T(\mathbf{r}') G^T(\mathbf{r}', \mathbf{r}; E') G^S(\mathbf{r} + \mathbf{R}, \mathbf{r}' + \mathbf{R}; E). \quad (6)$$

In eq. (6), $G^S(\mathbf{r}, \mathbf{r}'; E)$ and $G^T(\mathbf{r}, \mathbf{r}'; E)$ are the imaginary parts of the Green's function of the surface and tip defined by

$$G^S(\mathbf{r}, \mathbf{r}'; E) = \sum_{\mu} \phi_{\mu}^*(\mathbf{r}) \phi_{\mu}(\mathbf{r}') \delta(E - E_{\mu}), \quad (7)$$

$$G^T(\mathbf{r}, \mathbf{r}'; E) = \sum_{\nu} \phi_{\nu}^*(\mathbf{r}) \phi_{\nu}(\mathbf{r}') \delta(E - E_{\nu}), \quad (8)$$

respectively. The coordinate \mathbf{R} is a certain fixed point in the tip with respect to the frame work of the surface coordinate system, whereas \mathbf{r} is the internal one in the tip relative to the fixed point (Fig. 2.1).

The wave function of the surface decays into vacuum quite rapidly in proportion to the decay factor:

$$\gamma(z; E) = \exp(-z\sqrt{2m|E|}/\hbar), \quad (9)$$

where z is the distance from the surface and E is the energy of the electron measured from the vacuum level. Because the decay length is about 1 Å for most cases, the integral of eq. (6) is contributed almost from the very skin part of the tip extremity. Introducing a slowly varying factor of the surface Green's function

$$\tilde{G}^S(\mathbf{r}, \mathbf{r}'; E) = G^S(\mathbf{r}, \mathbf{r}'; E) \gamma^{-1}(z; E) \gamma^{-1}(z'; E), \quad (10)$$

and utilizing this fact, eq. (6) is rewritten as

$$A(\mathbf{R}, E, E') = \sum_{\nu} \int_{\Omega_T} d\mathbf{r} \int_{\Omega_T} d\mathbf{r}' V_T(\mathbf{r}) V_T(\mathbf{r}') \phi_{\nu}(\mathbf{r}) \phi_{\nu}^*(\mathbf{r}') \delta(E' - E_{\nu}) \\ \times \gamma(z; E) \gamma(z'; E) \tilde{G}^S(\mathbf{r} + \mathbf{R}, \mathbf{r}' + \mathbf{R}; E). \quad (11)$$

By a Taylor expansion of \tilde{G}^S about the point \mathbf{R} in this equation, we obtain

$$A(\mathbf{R}, E, E') = \left[\sum_{\nu} \left| \int_{\Omega_T} d\mathbf{r} V_T(\mathbf{r}) \phi_{\nu}(\mathbf{r}) \gamma(z; E) \right|^2 \delta(E' - E_{\nu}) \right] \rho(\mathbf{R}, E) \\ + \sum_m \sum_n \mu_{mn}(E') \nabla \dots \nabla \nabla' \dots \nabla' \tilde{G}^S(\mathbf{r}, \mathbf{r}'; E) \Big|_{\mathbf{r}=\mathbf{r}'=\mathbf{R}}. \quad (12)$$

In the above,

$$\mu_{mn}(E') = \int \mathbf{r} \dots \mathbf{r} \mathbf{r}' \dots \mathbf{r}' w(\mathbf{r}, \mathbf{r}'; E') d\mathbf{r} d\mathbf{r}', \quad (13)$$

is the moment of the weight function of the tip, which in turn defined by

$$w(\mathbf{r}, \mathbf{r}'; E') = V_T(\mathbf{r}) V_T(\mathbf{r}') \sum \phi_{\nu}(\mathbf{r}) \phi_{\nu}^*(\mathbf{r}') \gamma(z; E) \gamma(z'; E) \delta(E' - E_{\nu}). \quad (14)$$

Substituting expression (12) for the right-hand side of eq. (5), we finally

obtained the moment expansion of the tunneling current,

$$I = \frac{2\pi e}{\hbar} \int dE [f(E) - f(E + eV)] \left[\left[\sum_{\nu} \left| \int_{\Omega_T} d\mathbf{r} V_T(\mathbf{r}) \phi_{\nu}(\mathbf{r}) \gamma(z; E) \right|^2 \delta(E' - E_{\nu}) \right] \right. \\ \left. \times \rho(\mathbf{R}, E) + \sum_m \sum_n \mu_{mn}(E') \nabla \dots \nabla \nabla' \dots \nabla' \tilde{G}^S(\mathbf{r}, \mathbf{r}'; E) \Big|_{\mathbf{r}=\mathbf{r}'=\mathbf{R}} \right]. \quad (15)$$

Because the equation taking only the first term of this expression coincides with

TH equation (3), the TH approximation is valid when the higher order terms of

eq. (15) can be negligible. This would be the case only when the weight function

is concentrated in a narrow spatial region or when it is spherically symmetric.

As seen from its definition (eq. (14)), the weight function becomes negligible on

going inward and outward the tip in proportion to the decay factor and tip potential, respectively. Thus, if there is a tiny protrusion on the surface of the tip extremity, the weight function is almost localized there and the TH equation would be reasonable. There is, however, no reason to expect the higher order terms can be ignored for general cases, and eqs. (5) and (6) should be utilized for quantitative calculation of the tunnel current and STM simulation.

2.1.3. Thin organic layers

A thin organic layer adsorbed onto conducting substrate is one of the systems that has been extensively studied with STM because it represents a variety of surface phenomena and properties, such as corrosion, lubricant, and wetting. Hydrocarbons substituted by various functional groups have been observed with STM to know the appearance of the functional groups in STM images in addition to the aforementioned purpose. These studies revealed that some functional groups appear as bright features and the other as dark features in the images.^{1,9-11}

In general, it is often difficult to recognize functional groups on the basis of the strength of contrast in STM images. Functional groups of variously

substituted hydrocarbons exhibit either brighter or darker image contrast in their STM images than the alkyl moieties. The “bright” functional groups can be sufficiently discriminated themselves from the alkyl residues, and sometimes this allows structural analyses of the molecules or dynamic processes that the molecules exhibit.^{12,13} However, the “dark” functional groups cannot be recognized in the STM images because the substrate that is not covered with the adsorbates also appears as darker parts than the alkyl moieties in the images.

2.2. Molecular Tips^{14,15}

2.2.1. Analogy between electrochemistry and STM

Electrochemical methods traditionally have found important applications in sample analysis taking advantage of their great sensitivities toward measured currents. Simple metal electrodes, however, often encountered problems that hinder their applicability. The problems include undesired precipitation or adsorption and the slow reaction rates of sample species that lead one to apply overpotential for the desired electrochemical reactions. Since the mid-1970s, “tailored” chemical modification of electrodes

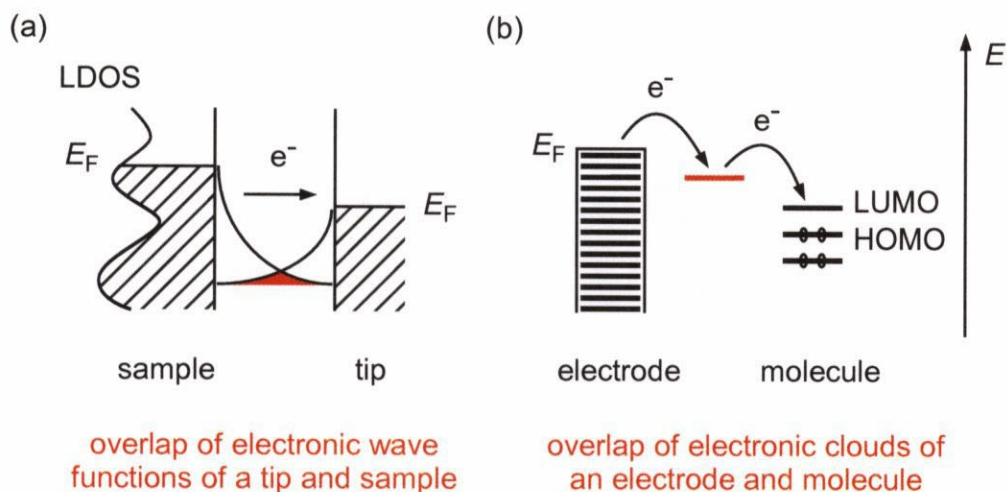


Fig. 2.2. Comparison of the energy diagrams for (a) electron tunneling in STM and (b) electron transfer at electrode surface in electrochemistry. The tip is positively biased in (a), and electrons tunnel from the sample to the tip. LDOS and E_F stand for local density of states and Fermi energy, respectively. Negative potential is applied to the electrode in (b), and electrons flow from the electrode to the LUMO of the molecule.

surface has been used. These chemically modified electrodes have not only overcome these problems but also enabled the control of the reaction rates and selectivities of electrochemical reactions. The selectivity frequently involves specific recognition of chemical species through chemical interactions, such as charge-charge and hydrogen bond interaction.¹⁶

Just as in electrochemistry, electron transfer plays an essential role in STM, which utilizes the electron tunneling as an operating principle.¹⁷ The electron tunnels through the overlap of electron wave functions of tip and sample surface as well as in electrochemistry (Fig. 2.2). This analogy in addition

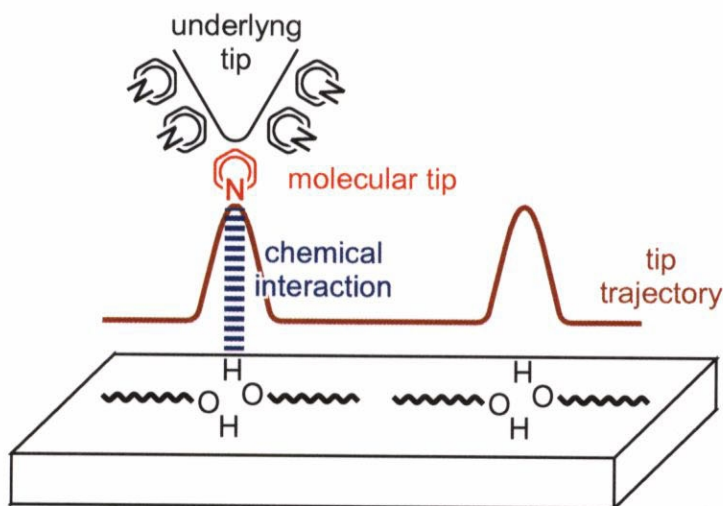


Fig. 2.3. Schematic illustration of STM observation with molecular tips. Chemical interaction between tip and sample molecules facilitates electron tunneling, so that the tip is retracted to keep the tunneling current constant in a constant current mode (brown line).

to the success of the chemically modified electrodes suggested that “tailored” chemical modification of STM tips should allow selective recognition of chemical species through rational use of chemical interactions (Fig. 2.3.).

2.2.2. Chemical modification of STM tips

Before our studies on molecular tips, it was reported that STM tips with atomic/molecular adsorbates at their apex, which were made either by accidental adsorption from gas phases^{18,19} or controlled micromanipulation,²⁰⁻²³ can affect image contrasts. In some cases the use of such tips allowed the discrimination of surface species.¹⁸⁻²³ The image

alterations with adsorbate-terminated tips have been explained alternatively by the changes in the electronic states of the tip^{18,20,22,24} or by tip-sample interactions.^{19,20,22-24} In contrast to these earlier studies, we prepared molecular STM tips by deliberate modification with chemically and functionally designed organic thin films. For instance, we employed self-assembled monolayers (SAMs) of thiols or conducting polymers for the tip modification. The chemical imaging was thereby obtained from a distinctive chemical affinity between tip and sample molecules that alters the tunneling current.

The molecular tips can be prepared by well-known and easy modification procedure. First of all, we prepare underlying gold tips by electrochemical etching in 3 M NaCl at ac 10 V, and cleaning in 7:3 concentrated H₂SO₄ : 30% H₂O₂. Simple immersion of the gold tips into 1–10 mM ethanolic solution of thiol (Fig. 2.4.) produces the SAM-modified tips.²⁵⁻²⁸ Polypyrrole films can be directly deposited onto gold tips by electrochemical polymerization of pyrroles, which was conducted by dipping the gold tips in aqueous or acetonitrile solutions containing electrolyte and pyrroles.²⁹ One should pay attention in washing the prepared polypyrrole-modified tips because pH of the solution significantly affects the observation of change in

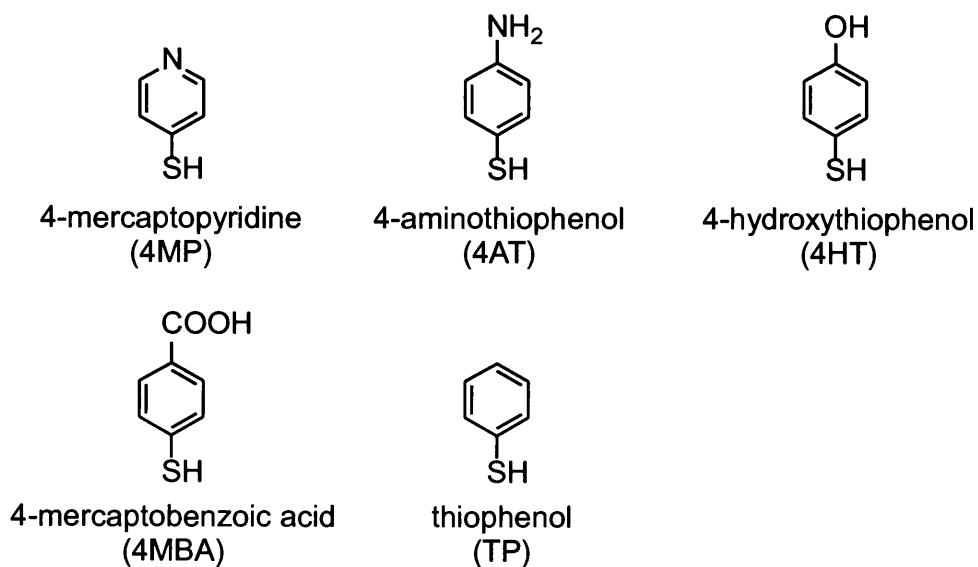
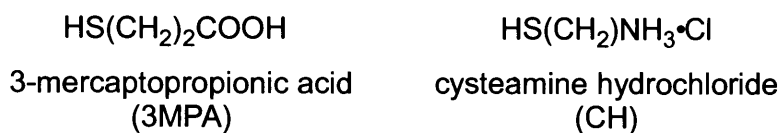
aromatic thiols*aliphatic thiols*

Fig. 2.4. Chemical structures of thiols used for the preparation of the molecular tips.

image contrast (see 2.2.5).²⁹

2.2.3. Discrimination of functional groups based on hydrogen bond interactions^{25,26}

In the first studies on the molecular tips, we examined how the tunneling current was affected by hydrogen bond interaction between the molecular tip and sample molecules, because it is known that rate constant of electron transfer is larger through hydrogen bonds than through σ bonds.³⁰ We

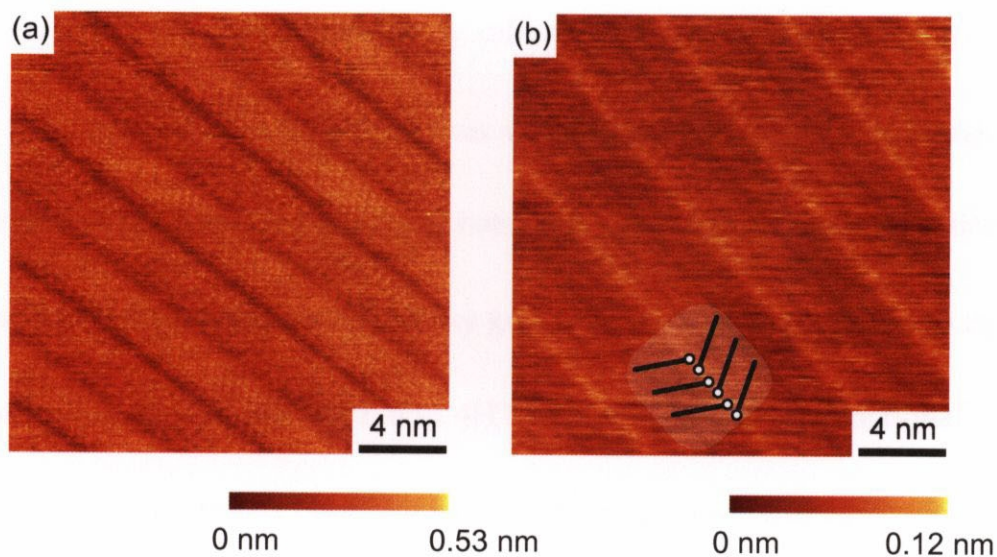


Fig. 2.5. STM images of stearyl alcohol ($\text{CH}_3(\text{CH}_2)_{17}\text{OH}$) physisorbed from a 1-phenyloctane solution onto HOPG: sample bias voltage -1.0 V (sample negative). (a) Observed with a gold tip: tunneling current 1.0 nA. (b) Observed with a 4-mercaptopyridine tip: tunneling current 0.7 nA. The molecular arrangement is schematically shown in the inset. Bars and circles represent alkyl moieties and hydroxy groups, respectively.

employed physisorbed monolayers of monosubstituted hydrocarbons on highly oriented pyrolytic graphite as the experimental systems. They are one of the most extensively studied samples by STM, and we can reproducibly obtain their STM images under ambient conditions.

Fig. 2.5a shows a typical STM image of stearyl alcohol ($\text{CH}_3(\text{CH}_2)_{17}\text{OH}$) physisorbed from a 1-phenyloctane solution onto HOPG as observed with a conventional gold tip. A herringbone structure consisting of parallel bright bands is seen. The bright bands correspond to individual sample molecules. Hydroxy groups, however, located on the end of stearyl alcohol cannot be

recognized in Fig. 2.5a. Significantly different images were observed with 4MP tips (Fig. 2.5b).²⁵ Parallel bright lines were observed in Fig. 2.5b, which were absent in Fig. 2.5a. The distance between the neighboring bright lines are consistent with that between hydroxy groups. Similar changes in image contrast were also observed with 4AT and 4HT tips, which contain functional groups available for hydrogen bond formation. Among them, the tip molecule that contains stronger hydrogen-bond basicity exhibited the contrast changes more frequently: the order of the basicity is pyridine (4MP) > aniline (4AT) > phenol (4HT). On the other hand, the contrast changes were not observed with gold and TP tips, which contain no functional groups for hydrogen bond. These results indicate that the bright lines correspond to the hydroxy groups of stearyl alcohol due to the facilitation of electron tunneling through hydrogen bond interaction between the molecular tips and the hydroxy groups of the sample molecules. Interestingly, molecular tips prepared with the aliphatic thiols, 3MPA and CH, gave no contrast change in spite of the presence of functional groups for hydrogen bond formation. The reason why only aromatic molecular tips changed the contrast in the STM images is not clear.

The molecular tips enabled selective recognition of carboxy groups as

well as hydroxy groups described above.²⁵ Again, 4MP and 4HT tips exhibited changes in image contrast selective to carboxy groups of stearic acid ($\text{CH}_3(\text{CH}_2)_{16}\text{COOH}$), whereas TP tips did not. These results further support the above conclusion that hydrogen bond interaction accounts for the changes in image contrast.

In the above examples, the tip molecules always interacted with the samples as hydrogen bond acceptors, and the hydrogen bond-donating functionality (hydroxy and carboxy groups) were selectively observed. Similar changes in image contrast were observed for ether oxygens.²⁶ Ether oxygens can form hydrogen bond only as hydrogen bond acceptor, and the tip molecules need to work as hydrogen bond donors to meet the requisite for hydrogen bond formation. Fig. 2.6 presents STM images of monolayers of dihexadecyl ether ($\text{CH}_3(\text{CH}_2)_{15}\text{O}(\text{CH}_2)_{15}\text{CH}_3$) on HOPG observed with (a) gold and (b) 4MBA tips. Fig. 2.6b shows bright lines separated by 4.1 ± 0.6 nm from each other, which is absent in Fig. 2.6a. As in the above examples, the change in image contrast was not observed TP tips, in which no functional groups are available for hydrogen bond interaction. The separation of the bright lines agrees with the intermolecular distance of the two ether oxygens of the

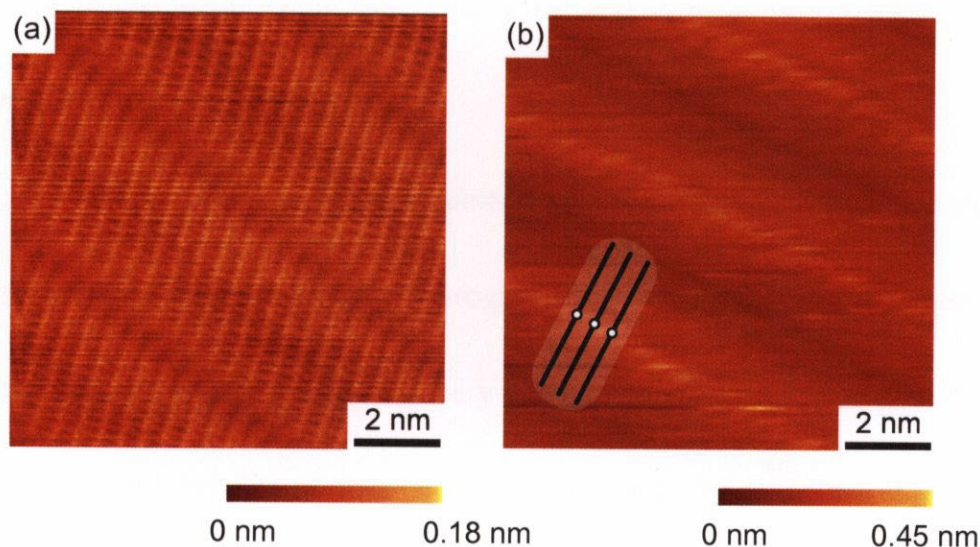


Fig. 2.6. STM images of dihexadecyl ether ($\text{CH}_3(\text{CH}_2)_{15}\text{O}(\text{CH}_2)_{15}\text{CH}_3$) physisorbed from a 1-phenyloctance solution onto HOPG: sample bias voltage 0.9 V (sample negative) and tunneling current 0.7 nA. Observed with (a) gold and (b) 4-mercaptobenzoic acid tip. Bars and circles represent alkyl moieties and ether oxygens, respectively.

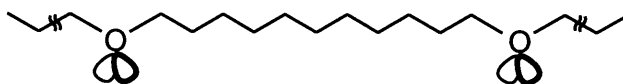
neighboring lamellae. These results suggest that the bright lines in Fig. 2.6b correspond to the position of the ether oxygens, and that the contrast change is attributed to hydrogen bond interaction with an acidic carboxy group of 4MBA molecule.

Unlike these three examples, no change in image contrast was observed for STM images of 1-chlorooctadecane ($\text{CH}_3(\text{CH}_2)_{17}\text{Cl}$) monolayers with molecular tips, such as 4MP or 4AT tips.²⁵ On the basis of all of the results described above, we conclude that molecular tips allow for chemically selective observation of functional groups that can form hydrogen bonds. The chemical selectivity is explained due to facilitation of electron tunneling through

overlapped electronic wave functions of tip and sample molecules brought by hydrogen bond interaction.

Not all molecular tips exhibited the chemically selective changes in image contrast originated from hydrogen bond, which can be explained by the absence of the tip molecules at the very extremity of the underlying gold tips. In addition, even when the contrast changes were initially observed with a certain molecular tip, the image was sometimes changed into the ones observed with unmodified gold tips after several-minutes' imaging under the identical condition. The loss of contrast changes may be due to removal of molecules from the underlying tip apex during scanning, as also suggested in earlier reports on tips with accidental adsorbates.¹⁸⁻²³

(a)



(b)

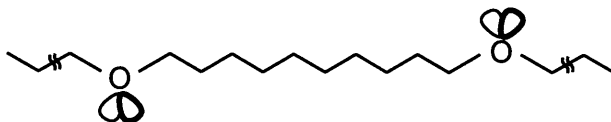


Fig. 2.7. Schematic illustration of the direction of two ether oxygens of (a) $C_{16}OC_{11}OC_{16}$ and (b) $C_{16}OC_{10}OC_{16}$ molecules in all-*trans* conformations.

2.2.4. Orientation-sensitive observation of ether oxygens²⁷

It is known that the strength of hydrogen bonds depends on the relative orientation of the hydrogen bond-donors and hydrogen bond-acceptors. The orientations of the functional groups that can form hydrogen bonds influence the strength of the hydrogen bonds between these functional groups and the molecular tips because different orientations result in a varying extent of orbital overlap. Consequently, we expected that enhanced contrasts resulting from hydrogen bond formation between sample and tip also depend on the molecular orientation and conformation of the sample molecules. To demonstrate this, we observed monolayers of diethers, $C_{16}H_{33}O(CH_2)_nOC_{16}H_{33}$ ($n = 10, 11$, hereafter abbreviated to $C_{16}OC_nOC_{16}$) with 4MBA tips, which allow discrimination of ether oxygens as bright contrast (see Fig. 2.6b). Importantly, the non-bonding oxygen orbitals point in the same direction in $C_{16}OC_{11}OC_{16}$ molecules (Fig. 2.7a), whereas they point in opposite direction in $C_{16}OC_{10}OC_{16}$ molecules (Fig. 2.7b).

Figs. 2.8a and 2.9a show STM images of $C_{16}OC_{11}OC_{16}$ and $C_{16}OC_{10}OC_{16}$ monolayers, respectively, as observed with gold tips. In both of the images, ether oxygens were observed darker than the alkyl residues of the molecules,

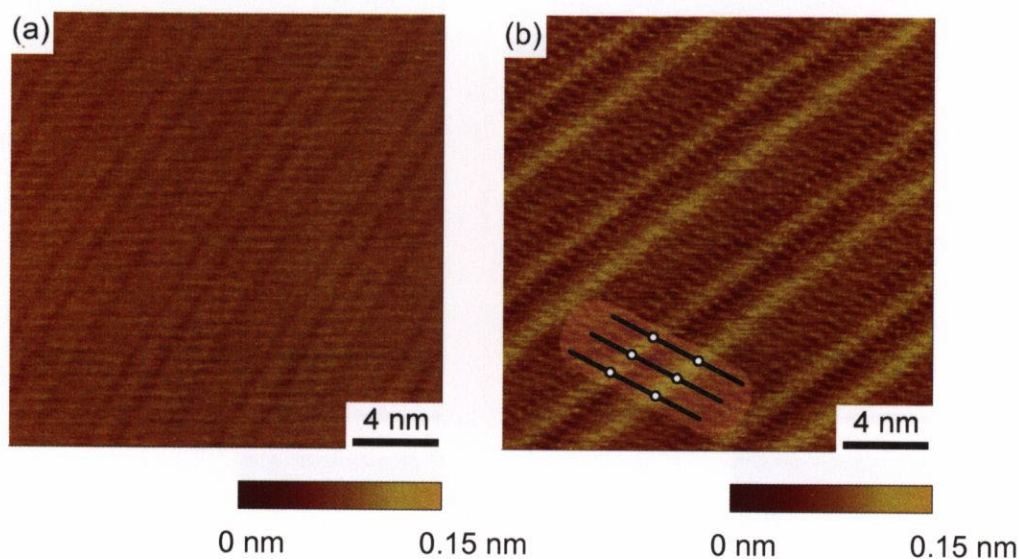


Fig. 2.8. STM images of $C_{16}OC_{11}OC_{16}$ monolayers physisorbed from 1,2,4-trichlorobenzene solution onto HOPG. (a) Observed with a gold tip: sample bias voltage 1.0 V (sample negative), and tunneling current 0.6 nA. (b) Observed with a 4-mercapto benzoic acid tip: sample bias voltage 0.8 V (sample negative), and tunneling current 0.5 nA. Bars and circles represent alkyl moieties and ether oxygens, respectively.

and it is difficult to discriminate them from the intermolecular troughs in the monolayers. In contrast, their STM images observed with 4MBA tips (Figs. 2.8b and 2.9b) exhibited pairs of bright lines, and the separation of the bright lines agrees with the distance of the two ether oxygens of the sample molecules. The bright lines were concluded to correspond to the ether oxygens on the basis of the geometrical consistency together with the previous results obtained with 4MBA tips (see 2.2.3). We attributed the changes in image contrast in Figs. 2.8b and 2.9b to the facilitation of electron tunneling through hydrogen bond interactions between ether oxygens of the samples and carboxy groups of 4MBA

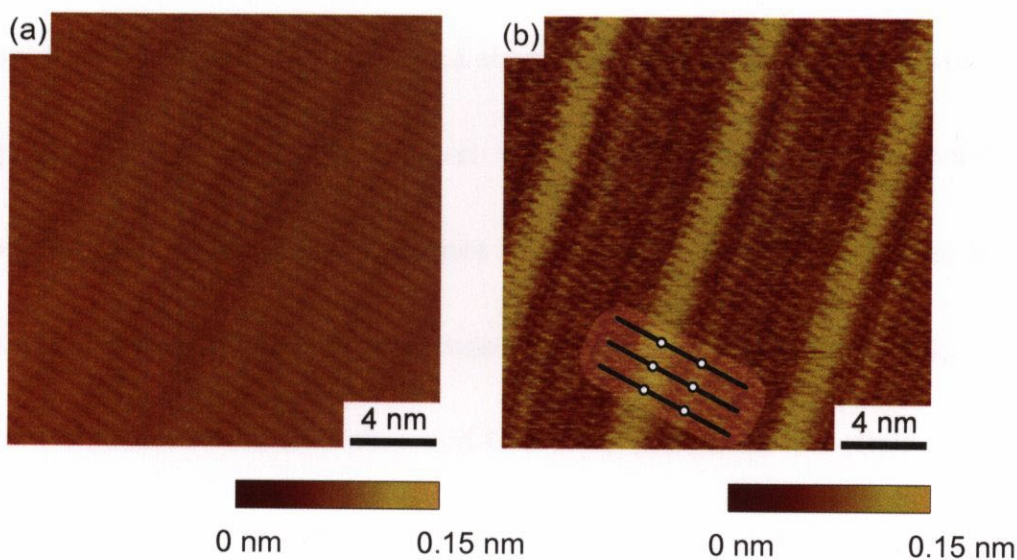


Fig. 2.9. STM images of $C_{16}OC_{10}OC_{16}$ monolayers physisorbed from 1,2,4-trichloro-benzene solution onto HOPG. (a) Observed with a gold tip: sample bias voltage 0.9 V (sample negative), and tunneling current 0.7 nA. (b) Observed with a 4-mercapto-benzoic acid tip: sample bias voltage 1.0 V (sample negative), and tunneling current 0.7 nA. Bars and circles represent alkyl moieties and ether oxygens, respectively.

molecules.

Interestingly, one bright line is much brighter than the other one for $C_{16}OC_{10}OC_{16}$ (Fig. 2.9b), while the two bright lines were equally bright for $C_{16}OC_{11}OC_{16}$ (Fig. 2.8b). This difference can be explained on the basis of orientation of these ether oxygens. In $C_{16}OC_{10}OC_{16}$ molecules in perpendicular orientation, the orbitals of one oxygen point down to the HOPG surface and the lone-pair orbitals of the second oxygen point up towards the STM tip. Because the orientation in which the donor and acceptor directly face each other is most favorable for hydrogen bond formation, the oxygen atom with the lone-pair

electrons pointing upwards can form a stronger hydrogen bond with 4MBA on the tip (Fig. 2.10a) than the oxygen with the lone-pair orbitals pointing downwards (Fig. 2.10b). This difference in the strength of the hydrogen bond causes the difference in the brightness for the two oxygens in Fig. 2.9b. Enhanced contrasts were also observed to a lesser extent for the ether oxygens pointing downwards to the HOPG surface, suggesting a hydrogen bond interaction between these oxygens and 4MBA on the tip, in spite of the unfavorable conformation of the oxygens (Fig. 2.10b). This weak hydrogen bond interaction may be explained by the fact that the lone-pair electron orbitals of these ether oxygens are oriented at an angle of approximately 55° relative to the surface normal when the carbon skeletal planes of the diethers are normal to the surface. In the case of $C_{16}OC_{11}OC_{16}$, the two ether oxygens point in the same direction and form hydrogen bonds with the same strength

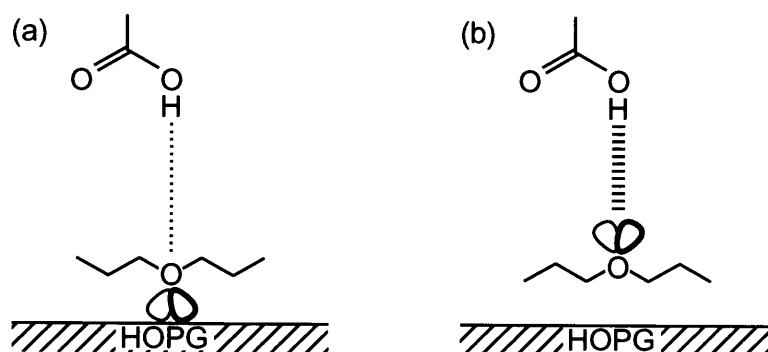


Fig. 2.10. Schematic illustration of the hydrogen bond interactions between carboxyl groups of 4MBA and ether oxygens in (a) unfavorable and (b) favorable orientation.

with the 4MBA on the tip. As a result, no difference in the brightness of the bright lines was observed in Fig. 2.8b.

This result strongly demonstrates that molecular tips make it possible to recognize not only the position but also the orientation of functional groups.

2.2.5. Polypyrrole tips²⁹

SAM-modified tips give rise to the facilitation of electron tunneling through hydrogen bond interactions between functional groups of tip and sample molecules. However, only a limited number of the tips (30% at most) allowed the observation of such selective change in electron tunneling. The preparation of the molecular tips utilized a conventional self-assembly process, which does not necessarily guarantee the presence of the tip molecules at the very apex of the underlying gold tips. This probably explains the occasional failure in the facilitated electron tunneling.

Drawing once more an analogy to chemically modified electrode (see also 2.2.1), we wondered whether use of polymer-modified tips could improve the experimental reproducibility.²⁹ Polymer films are often used as electrode coating and, due to their chemical and electrochemical stability, can

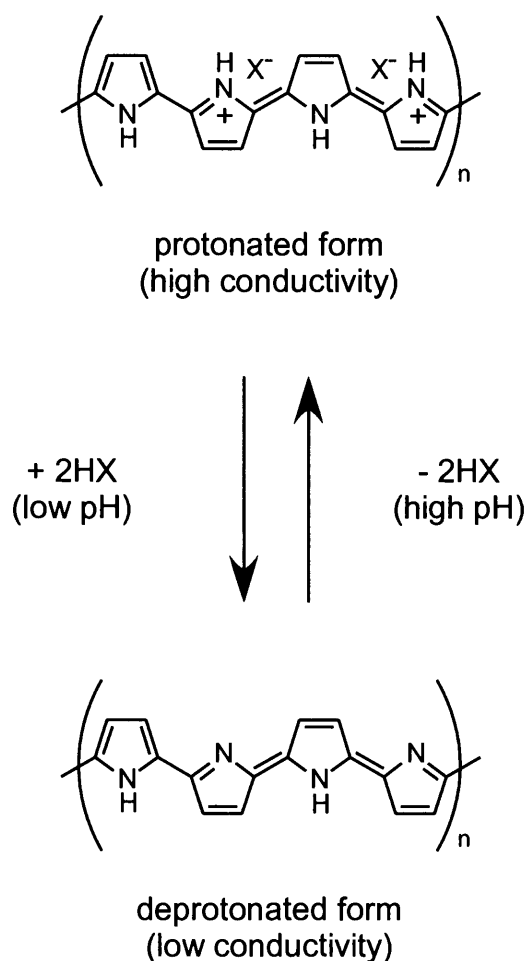


Fig. 2.11. Effect of pH on the protonation/deprotonation of polypyrroles.

considerably improve the reproducibility of electrochemical experiments.¹⁶ We employed conducting polypyrrole as a tip molecule due to its high stability and the feasibility of its reproducible preparation. Most importantly, polypyrrole can form hydrogen bonds through its nitrogen moieties. The polypyrrole tips indeed exhibited changes in image contrast selective to hydroxy and carboxy groups of 1-alkanol and 1-alkanoic acid monolayers, respectively. The proportion of tips that exhibited the contrast changes to the examined tips

strongly depended on how polypyrrole tips were washed after the electrochemical polymerization. The proportion was higher for the tips washed at pH 7 than for those washed at pH 5.5 and 6, and was very small for those washed at pH 2. It is known that the NH moiety of polypyrrole subunits gradually deprotonates with increasing the pH of a solution in which polypyrrole is immersed. The above tendency thus means that basic, deprotonated polypyrrole subunits (Fig. 2.11) involve the contrast change of the hydroxy and carboxy groups like the SAM-modified tips (see 2.2.3). In addition, the proportion was higher for the polypyrrole tips (50% at most) than for SAM-modified tips.

2.2.6. Discrimination of metal ions of porphyrins based on metal-coordination and hydrogen bond interactions²⁸

In the above, the chemical recognition is attained by facilitation of electron tunneling through hydrogen bond interaction between tip and sample molecules. The overlap of molecular orbitals of these molecules plays an essential role in the facilitation, and chemical interactions other than hydrogen bonding, such as metal-coordination interaction, can provide the electronic

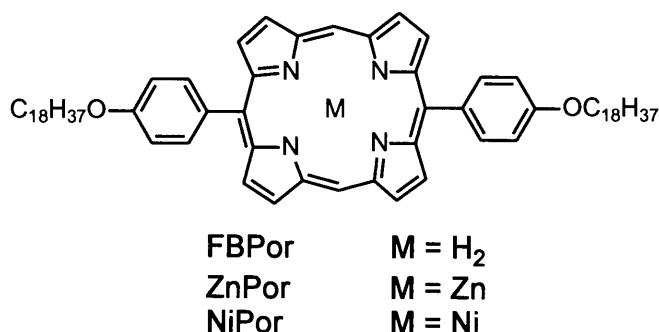


Fig. 2.12. The chemical structures of the porphyrins used for the STM observation. coupling. We therefore extended the idea of the molecular tips toward metal-coordination interaction.

Porphyrins diagonally substituted with long alkyl chains at the two *meso* positions (Fig. 2.12) were used as samples. The porphyrins adsorbed onto HOPG surface through their alkyl chains to form monolayers, and molecularly resolved images were observed. When gold tips were used for the observation, the centers of all of the porphyrins were observed as depressed compared with the pyrrole moieties irrespective of the presence or absence of the central metal ions. In addition, the pyrrole moieties were observed as protrusion and their brightness (height) was almost the same for all of the porphyrins. These porphyrins as a result cannot be discriminated from each other with gold tips.

In contrast, significantly different images were observed with 4MP tips, whose pyridine nitrogens can form hydrogen bond and coordination bond with

the pyrrole hydrogens and the metal ions, respectively, at the center of the porphyrins. Although the pyrrole moieties were observed as elevated as compared with alkyl residues, centers of the porphyrin rings were further protruded over the pyrrole moieties.

Two kinds of the bright spots were observed for mixed monolayers of ZnPor and NiPor (Fig. 2.13). Both of the spots were brighter than the porphyrin rings, but one spot is brighter than the other one. The ratio of the number of the former to that of the latter is approximately 2 to 1, which is the same as the molar ratio of ZnPor to NiPor in the solution used for physisorption. The ratio of the brighter spots observed with 4MP tips increased with increasing the

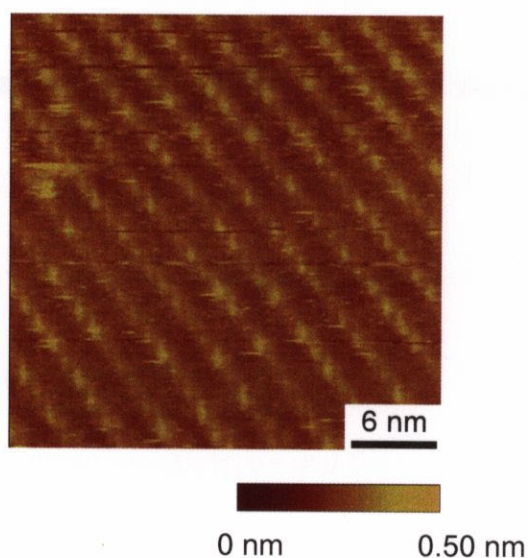


Fig. 2.13. STM image of a mixed monolayer of ZnPor and NiPor (2:1) physisorbed from a 1,2-dichlorobenzene solution onto HOPG. Observed with a 4 mercaptopyridine tip: sample bias voltage 1.1 V (sample negative), and tunneling current 0.32 nA.

molar ratio of ZnPor in sample solutions. In addition, the heights of the brighter spots and the other one were consistent with those of the central bright spots in STM images of pure monolayers of ZnPor and NiPor, respectively, observed with 4MP tips. These results indicate that the former and the latter spots correspond to central metal ions of ZnPor and NiPor, respectively. It is well known that axial coordination of neutral ligands such as pyridine to metalloporphyrins is much stronger for zinc porphyrin than for nickel porphyrin. The difference of the contrasts of the porphyrin centers probably reflects the magnitude of the metal-coordination interaction between the pyridine nitrogen of 4MP tips and the central metal ions of the porphyrins.

These results demonstrate that metal-coordination interaction as well as hydrogen bond interaction is available for chemical recognition attained with the molecular tips.

3. A Fullerene Molecular Tip: Locating Electroactive Moieties and a Novel Intermolecular Junction for Molecular Electronics

3.1. Introduction

Scanning tunneling microscopy (STM) provides a means for revealing a real space view of single atoms and molecules on a conducting substrate. In addition, STM and its related technique, scanning probe microscopies (SPMs), also makes it possible to probe electronic conductivity of the visualized single molecules or particular moieties within these molecules in nanoenvironment.³¹ The evaluation of the electronic conductivity of individual molecules is critical for realization of molecular electronics, in which single or small groups of molecules are utilized to perform electronic functions.³²

We have studied on the use of molecular tips instead of conventional metal tips for STM imaging. The molecular tips are prepared by chemical modification of underlying metal tips, and the outermost single molecular adsorbate probes intermolecular electron tunneling to or from a sample molecule. Importantly, the tunneling current increases when sample and tip

molecules form a chemical interaction that provides overlap of electronic wave functions between them. The current increase is ascribed to the facilitated tunneling through the overlapped electronic wave functions. We have demonstrated that this phenomenon can be utilized for selective observation of chemical species to overcome poor chemical selectivity in conventional STM.^{25-29,33,34} For example, 4-carboxythiophenolate tips have been used for ether-oxygen selective observation based on a hydrogen bond interaction between the carboxy group of the tip and the ether oxygens of sample molecules,^{26,27} or 4-pyridinethiolate tips for metal-ion selective observation based on a metal-coordination interaction between the pyridine nitrogen of the tip and metalloporphyrins.²⁸ Because the overlap of electronic wave functions is important for the facilitation of intermolecular electron tunneling between tip and sample, these results suggest that the electron tunneling should be facilitated also through the remaining electronic interaction, namely, a charge-transfer interaction in addition to the hydrogen bond and metal-coordination interactions. Electron donors and acceptors, which form charge-transfer interaction with each other, constitute major components for molecular electronic devices, such as molecular wires, diodes, or switches.³²

Both the spatial arrangement of the electroactive species and their electronic configuration within the local environment are key factors to realize the device functions in a desired manner.

We herein demonstrate that molecular tips allow us to pinpoint electron-donaing or -accepting moieties in single molecules based on facilitated electron tunneling through charge-transfer interaction. In addition, we observed asymmetric electron transport between donor and acceptor, indicating the possibility for the molecular tip to address the electronic properties of donor–acceptor assemblies.

Molecular tips possessing a fullerene moiety was used for STM observation of physisorbed monolayers of free-base porphyrin and metalloporphyrins (Fig. 3.1a) onto highly oriented pyrolytic graphite (HOPG).

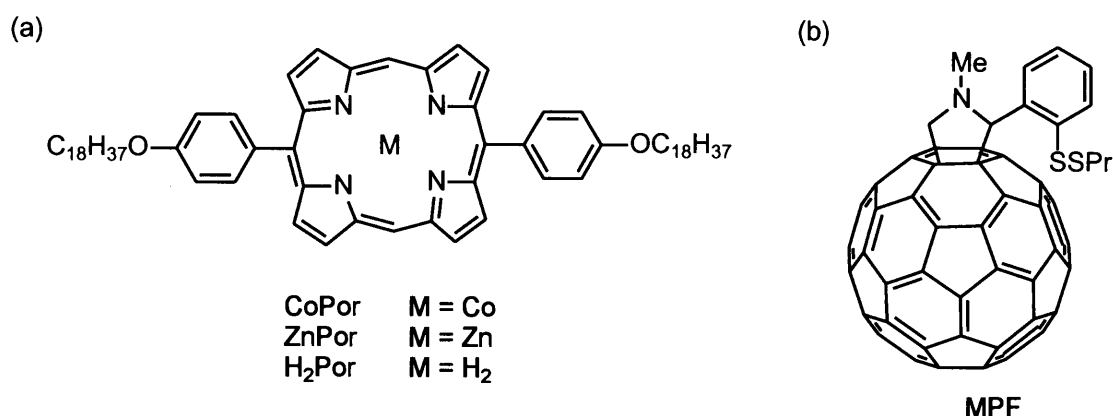


Fig. 3.1. Chemical structures of the (a) sample and (b) tip-modifying molecules along with their abbreviations.

They were prepared from a fullerene derivative, *N*-methyl 2-(2-propyldithiophenyl)fulleropyrrolidine (MPF, Fig. 3.1b), by self-assembly through its disulfide group onto an underlying gold tip (Fig. 3.1c). Porphyrins are one of the most frequently employed building blocks as electron acceptors for photoinduced electron transfer in supramolecular systems,³⁵ and fullerenes show facile electron acceptability.^{36,37} Therefore, the combination of porphyrins and fullerenes offers single molecular assemblies suitable for studying intermolecular electron tunneling between them.

3.2. Experimental Section

3.2.1 General

All reagents were of the highest grade available and used as received. Sarcosine and 1,2,4-trichlorobenzene were purchased from Wako Pure Chemical (Osaka, Japan), and fullerene was from Tokyo Kasei Kogyo (Tokyo, Japan). De-ionized water purified with a Milli-Q water purification system (Japan Millipore, Tokyo, Japan) was used throughout the experiments. STM observation was performed on a Nanoscope E (Digital Instrument, Santa

Barbara, CA) at ambient temperature under air.

3.2.2. Synthesis of *N*-methyl 2-(2-propyldithiophenyl)fulleropyrrolidine (MPF)

Sarcosine (0.892 g, 10.0 mmol), C₆₀ (0.729 g, 1.01 mmol), and 2-propyldithiobenzaldehyde (0.214 g, 1.01 mmol) were dissolved in argon-saturated toluene (800 ml). The reaction mixture was refluxed for 4 h under a nitrogen atmosphere and dark. The solution was cooled at rt and evaporated to dryness under reduced pressure. The crude product was purified by flash column chromatography over silica gel with toluene/hexane (1/2) as eluent to give 0.230 g of the fullerene derivative (24%).

3.2.3. STM tip preparation

Tips made of Pt/Ir (Digital Instruments) were used for the STM observation of MPF SAMs. Gold tips were used for the observation of physisorbed monolayers of porphyrin derivatives. Small pieces of gold wire (0.25 mm diameter, Nilaco Co., Tokyo, Japan; 99.95%) were electrochemically etched in 3 M NaCl at AC 10 V. They were washed by sonicating in pure water

and further dipping in “piranha solution” (7:3 concentrated $\text{H}_2\text{SO}_4/\text{H}_2\text{O}_2$.

Caution: piranha solution reacts violently with organic compounds and should not be stored in closed containers), and finally washed thoroughly with pure water. MPF was dissolved in argon-saturated toluene at the typical concentration of 20 μM , and gold tips were immersed in the solution overnight for the SAM formation. The modified tips were successively rinsed with toluene and water prior to use.

3.2.4. STM observation of MPF SAMs

Gold films deposited onto mica substrates were purchased from Platypus Technologies (Madison, WI). The Au films were thoroughly washed with water and annealed with hydrogen flame to improve their flatness and orientation, and modified with MPF similar to the tip modification (see above). After drying under argon stream, the MPF-modified Au films were observed with STM typically with a bias voltage of -1.8 V and a tunneling current of 0.17 nA.

3.2.5. STM observation of physisorbed monolayers of the porphyrins

CoPor (Fig. 3.1a) was dissolved in 1,2,4-trichlorobenzene at a

concentration of 0.5 mg/ml. ZnPor and FBPor (Fig. 3.1a) were codissolved in 1,2,4-trichlorobenzene at a molar ratio of 1:3 and total concentration of 1.0 mg/ml. Either one of the solutions was applied onto a basal plane of freshly cleaved highly oriented pyrolytic graphite (HOPG). Within minutes after the deposition of the solution, STM observations were performed at the solution/HOPG interface typically with a bias voltage of -1.2 to -1.5 V and a tunneling current of 0.3 – 0.5 nA.

3.3. Results

3.3.1. Tip modification

The MPF molecule used for the tip modification contains a fullerene-containing moiety, a propyldisulfanyl group, and a phenylene bridge between them (Fig. 3.1b). Because of the large van der Waals diameter of the fullerene moiety (about 1 nm), SAMs of fullerene derivatives tethered with single thiol-containing alkyl chains would have low packing density. Stable modification of STM tips is crucial for highly reproducible chemically selective observation, and well-packed SAMs are ideal for this. We thus chose the

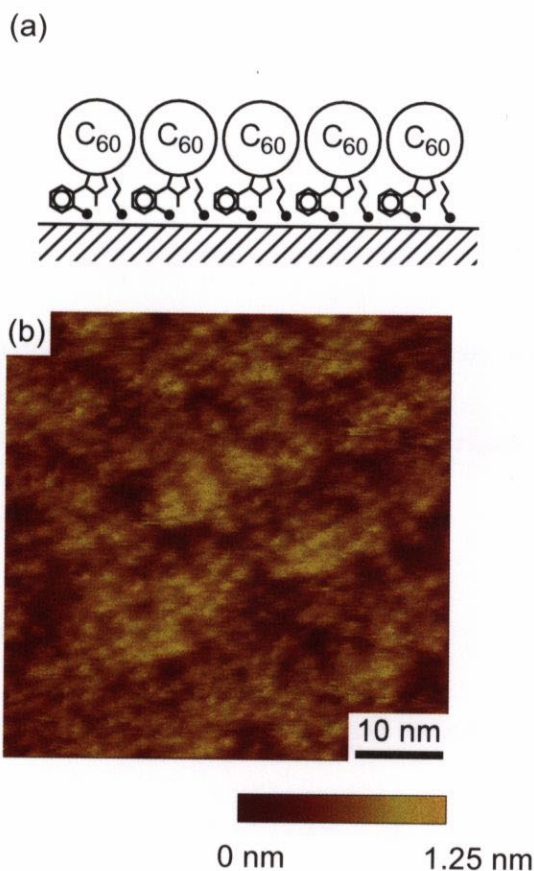


Fig. 3.2. (a) A schematic illustration of MPF SAMs on gold surface. The nitrogen atoms of pyrrole ring are omitted, and the sulfur atoms of the thiolates are represented by solid circles for simplicity. (b) An STM image of MPF-modified gold surface. Bias voltage, -1.70 V; tunneling current, 0.17 nA.

disulfide bond for the SAM formation.^{38,39} Two kinds of thiolates are formed upon the chemisorption of MPF on gold surfaces. One is the propyl thiolate, and the other is the remaining part of the MPF molecule. The former would contribute to increase the packing density, which gives rise to well-packed SAMs terminated with fullerene moieties (Fig. 3.2a).

MPF SAMs formed on Au (111) were observed with STM using Pt/Ir tips to evaluate their quality. Fig. 3.2b shows a representative STM image of

MPF SAMs, in which many circular protrusions were observed all over the surface. Their sizes are around 1 nm, and this value corresponds well to the van der Waals diameter of a pristine fullerene molecule measured by STM observation.⁴⁰ Although no ordering of the fullerene moieties was discerned, Fig. 3.2b demonstrates their high coverage on the surface.

3.3.2. CoPor monolayer

First, a CoPor monolayer was observed to investigate how the fullerene derivative tip affects the tunneling current. Fig. 3.3a shows an STM image of CoPor monolayer observed with a gold tip, in which ordered arrays of porphyrin rings were observed. The measured diameter of the rings and their separation between the neighboring rows in Fig. 3.3a agree with the diameter of the porphyrin ring and length of the octadecyl side chain, respectively, as estimated from a CPK model.²⁸ The porphyrin rings of CoPor was observed as having central protrusions when gold tips were used, which is clearly seen in its cross sectional profile (Fig. 3.3a, bottom). The protrusions are assigned to the central cobalt(II) ions of CoPor molecules. This can be interpreted as large tunneling probability associated with half-filled d_{z^2} orbital of the cobalt(II)

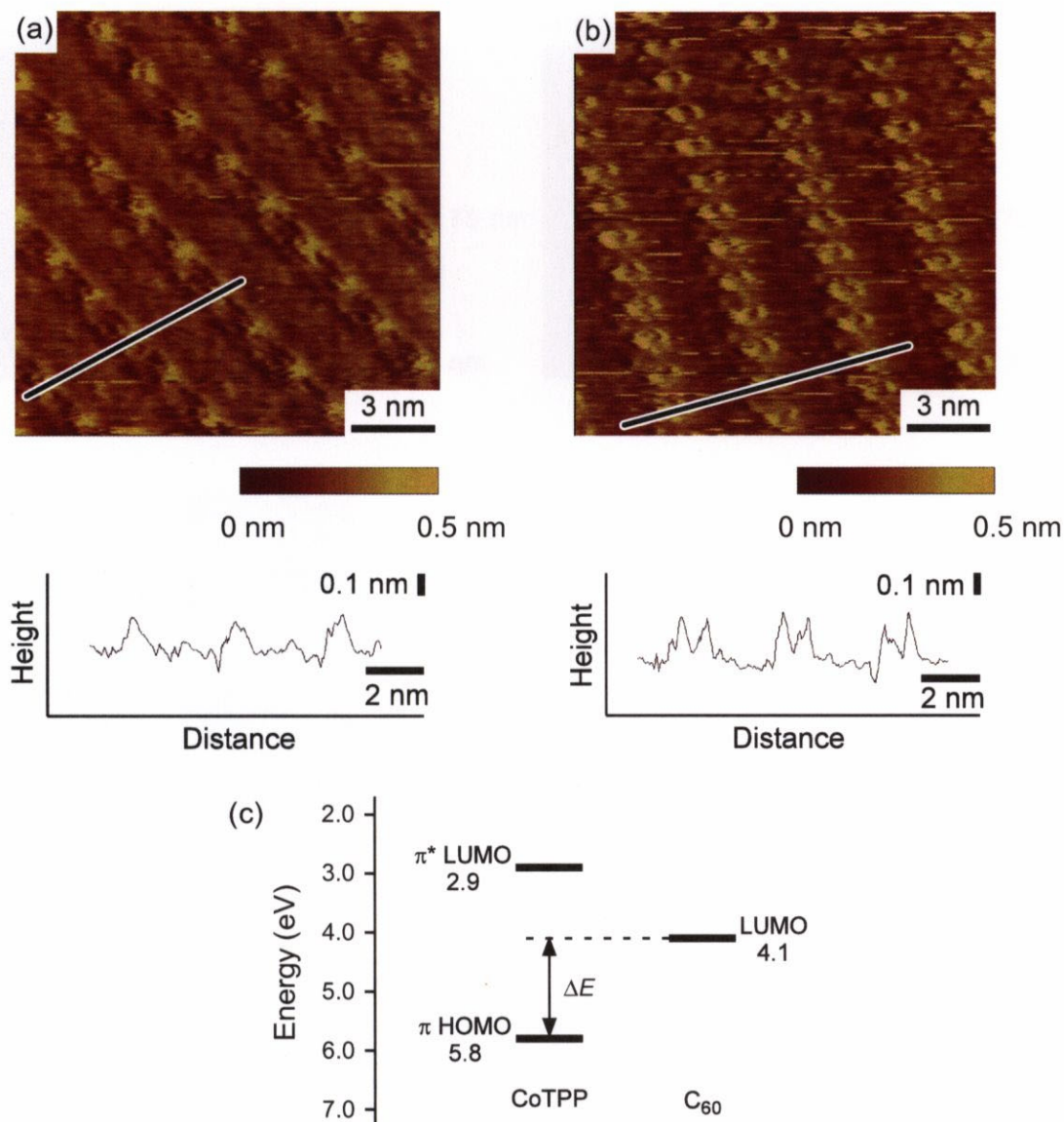


Fig. 3.3. STM images of CoPor monolayers physisorbed onto HOPG. The cross-sectional profiles measured along with the lines in the STM images were presented below. (a) Observed with a gold tip: sample bias voltage, -1.30 V (sample negative); tunneling current, 0.30 nA. (b) Observed with a MPF tip: sample bias voltage, -1.25 V; tunneling current 0.30 nA. (c) An energy diagram of cobalt(II) tetraphenylporphyrin (CoTPP) and fullerene (C₆₀).

ion.⁴¹

When MPF tips were used for the observation of CoPor monolayers, significantly different images were observed (Fig. 3.3b). The STM image

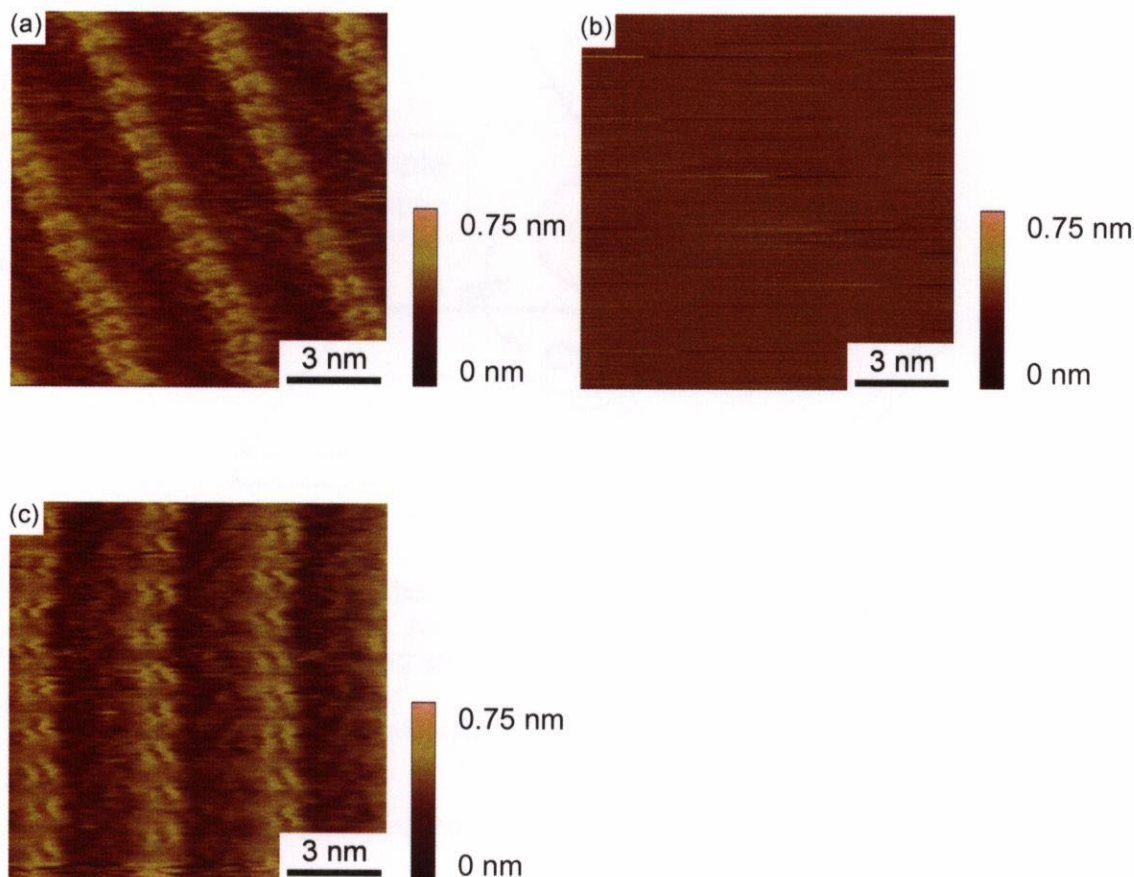


Fig. 3.4. STM images of CoPor monolayer physisorbed onto HOPG observed with MPF tips. Tunneling current, 0.30 nA; bias voltage (a) 1.35 V (sample negative), (b) +1.20 V (sample positive), and (c) 1.35 V (sample negative). These images were successively observed with the same tip and within the same sample region. After the acquisition of (b) and changing the polarity to sample negative again, the physisorbed monolayer under observation began to reorganize. As a result, the monolayer orientation in (c) was different from that in (a).

exhibited periodically aligned porphyrin rings as circular protrusions having central depressions, whose geometries are consistent with those estimated from a CPK model. The most striking difference between Figs. 3.3a and 3.3b is the image contrast of the pyrrole moieties surrounding cobalt(II) ions. These moieties were observed dimmer than the metal ions when gold tips were used (Fig. 3.3a). However, they appeared as protrusions relative to the cobalt(II) ions

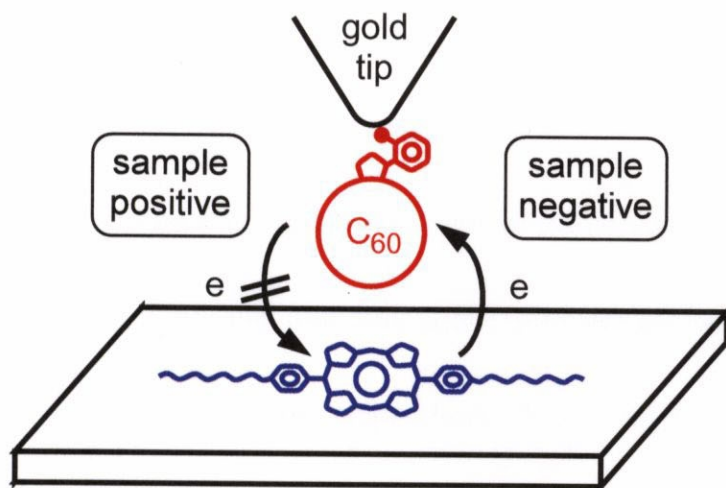


Fig. 3.5. Schematic illustration of electron flow between a porphyrin (blue) and fullerene-derivative (red) tip. All the atomic labels were omitted for simplicity in the chemical structures of tip and sample molecules.

in the STM images observed with MPF tips (Fig. 3.3b). We observed the change in image contrast selective to the porphyrin rings when the sample was negatively biased. The contrast change was not dependent on the magnitude of the bias voltage with the range of -1.2 V to -1.5 V, and below or above this range no clear molecular image was observed. Interestingly, with MPF tips we observed entirely flat STM images that exhibited no circular protrusion of the porphyrin ring when the sample was positively biased, and the contrast change was restored upon reversing the polarity where the sample was negatively biased (Fig. 3.4). These results indicate that the electron tunneling is favored in the direction from the porphyrin to the fullerene derivative but suppressed in the opposite direction (Fig. 3.5).

3.3.3. Mixed monolayer of FBPor and ZnPor

Next, we observed a mixed monolayer of ZnPor and FBPor with the fullerene derivative tip. Figs. 3.6a and 3.6b show STM images of the monolayer observed with a gold and MPF tips, respectively. Again, the bright protrusions in both of the images are assigned to the porphyrin rings because their geometries are in agreement with those of a CPK model.²⁸ The sample solution, from which the observed porphyrins were adsorbed onto HOPG surface, contains two kinds of porphyrins with and without a central metal ion. Nevertheless, the centers of all the porphyrin rings were observed as depressed compared to the surrounding pyrrole moieties in Fig. 3.6a. It is natural for the centers of porphyrin rings of FBPor to be observed as depressed because central metal ions are absent in FBPor. The d_{z^2} orbitals of zinc(II) ions of ZnPor are fully filled unlike the case in CoPor, which results in little tunneling current at the central metal ions of ZnPor. This presumably accounts for the depressed appearance of the centers of porphyrin rings of ZnPor.⁴¹ In addition, all the porphyrin rings were observed at similar image contrast, and as a result the two species that should coexist on the surface cannot be discriminated from each

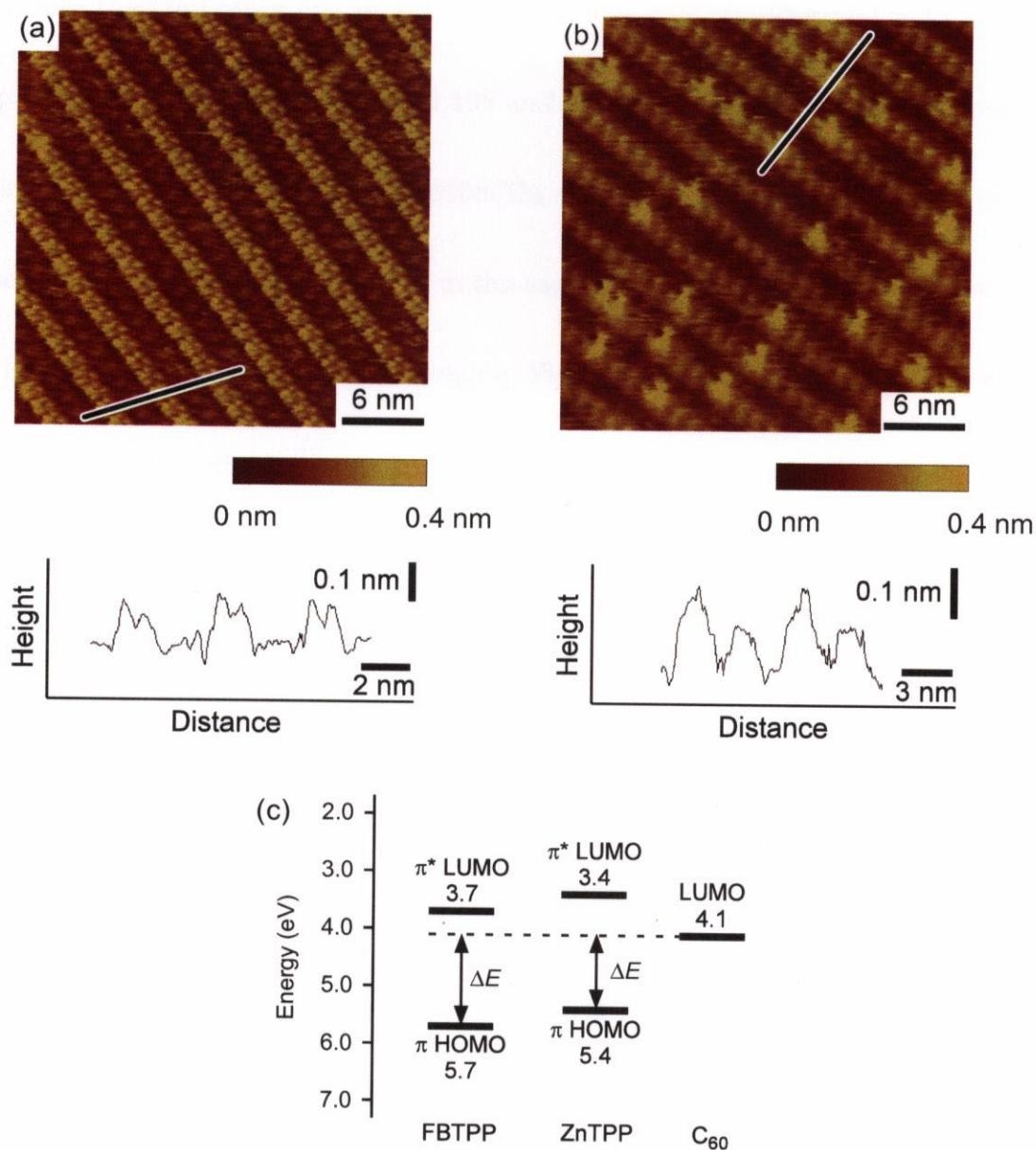


Fig. 3.6. STM images of mixed monolayers of FBPor and ZnPor physisorbed onto HOPG. The cross-sectional profiles measured along with the lines in the STM images were presented below. (a) Observed with an unmodified gold tip: sample bias voltage, -1.20 V; tunneling current, 0.35 nA. (b) Observed with a MPF tip: sample bias voltage, -1.30 V; tunneling current, 0.45 nA. (c) An energy diagram of free-base and zinc(II) tetraphenylporphyrin (FBTTP and ZnTTP, respectively) and fullerene (C₆₀).

other.

In strong contrast to Fig. 3.6a, one porphyrin ring was observed much

brighter than the other one in Fig. 3.6b. In a wider image observed with a MPF tip (data not shown), there existed 108 and 326 rings with brighter and dimmer contrast, respectively. Their ratio ($108/326 = 1.0/3.0$) is in exact agreement with the molar ratio of ZnPor to FBPor in the sample solution. This suggests that the brighter and dimmer porphyrin rings in Fig. 3.6b correspond to those of ZnPor and FBPor, respectively.²⁸

3.4. Discussion

3.4.1. Imaging mechanism

Recent studies have shown that a fullerene forms supramolecular complexes with both a free-base porphyrin and metalloporphyrins.⁴² Although the nature of the fullerene–porphyrin interactions is still not fully understood, it is widely suggested that charge-transfer or π - π interactions account for the supramolecular assembly.⁴³⁻⁴⁵ On the other hand, we have observed the facilitation of electron tunneling based on the interactions that bring overlap of electronic wave functions of sample and tip molecules.^{25-29,33,34} These studies indicate that the changes in image contrast observed with MPF tips (Fig. 3.3b)

are due to the charge-transfer interaction concomitant to the overlapped π orbitals between a fullerene moiety of the MPF molecule and porphyrin rings of the CoPor molecules. The porphyrin rings were observed as brighter contrast than the cobalt(II) ions when MPF tips were used (Fig. 3.3b) due to facilitation of electron tunneling through the overlapped wave functions. Because porphyrins and fullerenes are electron-rich and -deficient, respectively, the charge-transfer interaction between them involves the highest occupied π molecular orbital (π HOMO) of CoPor and lowest unoccupied molecular orbital (LUMO) of the fullerene derivative. The former and the latter are high and low in energy, respectively, and this energy relation should allow electron to flow only in one direction with a finite applied voltage (Fig. 3.3c). The observed polarity dependence thus indicates that the facilitated electron tunneling at pyrrole moieties of CoPor involves the charge-transfer interaction with the fullerene moiety of the tip molecules.⁴⁶

The difference in image contrast of FBPor and ZnPor in Fig. 3.6b emphasizes the importance of the charge-transfer interaction for the facilitation of electron tunneling. Although a free-base porphyrin binds a fullerene more strongly than a metalloporphyrin,⁴⁷ it has been theoretically predicted that the

charge-transfer interaction is greater for fullerene/metalloporphyrin than for fullerene/free-base porphyrin.⁴⁸ The difference in the extent of the charge-transfer interaction is also evident by considering the difference in energy between π HOMOs of FBPor and ZnPor. The energy of π HOMO of zinc(II) tetraphenylporphyrin is reported to be 0.3 eV above that of the free-base derivative.⁴¹ The zinc(II) derivative is thus expected to have favorable charge-transfer interaction with the fullerene derivative compared with the free-base derivative, because the π HOMO of the former is energetically closer to the LUMO of fullerene than the latter (Fig. 3.6c). The favorable charge-transfer interaction between the fullerene and ZnPor facilitates electron tunneling to a great extent as compared with the interaction of fullerene/FBPor, which results in the brighter appearance for ZnPor in Fig. 3.6b. We conclude that molecular tips are capable of detecting electron-donating or -accepting moieties in single molecules based on charge-transfer interactions. Moreover, it is demonstrated that different electron donors (acceptors) can be discriminated according to the energy levels of their π orbitals involved in the interaction with the tip molecule.

3.4.2. Polarity dependence

Besides the chemical selectivity, the polarity dependence is another noteworthy aspect from the viewpoint of characterization of molecular devices. Aviram and Ratner have proposed a molecular rectifier of donor–acceptor species, which is an organic analogue of a solid-state p – n junction diode.⁴⁹ Although great experimental progress has been made since its proposal in 1970s, experimental difficulties still prevent characterization of its rectifying behavior at a molecular level.³² The present tunnel junction consists of the electron-rich porphyrin and electron-deficient fullerene facing and interacting each other (Fig. 3.5), and can be regarded as the molecular rectifier. The diode nature of the tunnel junction is evident from the polarity dependence discussed above. The measurement of current–voltage (I – V) characteristics can give more insight into the electron transport mechanism of the molecular diodes. The I – V measurement in an argon atmosphere in fact revealed the rectification behavior where the current was driven only at sample-negative bias. Quantitative characterization of the rectification would be possible by further elaboration of the experimental system, employing the same metal material for underlying tip and substrate to make the upper and lower halves of the junction (Fig. 3.5)

symmetric except the fullerene and porphyrin molecules. These results indicate that molecular tips are potentially applicable to measuring intermolecular electron transport within a single molecular assembly that consists of one molecule on the tip and another molecule on a conducting substrate. By constructing a molecular electronic device with the assembly between a tip and substrate, the measurement would reveal the electronic behavior of the device, such as rectification behavior of a molecular diode preliminary shown in this report, that cannot be addressed with conventional metal tips.

3.5. Conclusions

In summary, it was revealed that electron tunneling is facilitated through a charge-transfer interaction between a fullerene-derivative STM tip and porphyrins on HOPG surface. We conclude that molecular tips provide a means for locating electron-donating or -accepting moieties in single molecules based on the facilitated tunneling through charge-transfer interactions. In addition, the tunnel junction, consisting of the fullerene derivative and porphyrin, can be regarded as a molecular diode, and the rectification behavior was in fact observed. We believe that molecular tips can construct novel

intermolecular junctions suitable for testing molecular electronic devices.